1. Literature review of H-atom abstraction and $RONO_2$ formation branching ratios

At the core of understanding the source of C_1-C_5 $RONO_2$ in the atmosphere is a clear understanding of the branching ratios relevant to their production. Below, we summarize the current state of knowledge of these branching ratios. Table S1 summarizes the branching ratios for H-atom abstraction (α_1) in the OH + alkane reactions used for the $RONO_2$/RH model below. The values of α_1 were calculated using the structural activity relationship partial rate constant method detailed in Kwok and Atkinson (1995). We tested the sensitivity of the branching ratio values to the difference in the winter 2011 average daytime temperature (278 K) and the summer 2015 average daytime temperature (298 K), and found no change in values over the small temperature range.

Table 5 presents a summary of branching ratios for $RONO_2$ formation (α_3, R3b) in recent and past literature for the C_3-C_5 $RONO_2$ and Table 3 for $MeONO_2$ and $EtONO_2$. The list of references in both tables are not exhaustive, but highlight the major studies that have been used to interpret $RONO_2$ observations previously (e.g. Bertman et al., 1995; Reeves et al., 2007; Russo et al., 2010; Simpson, 2003; Sommariva et al., 2008; Wang et al., 2013; Worton et al., 2010). These studies have experimental or calculated branching ratios at, or extrapolated to, temperatures and pressure relevant to the lower atmosphere. The $RONO_2$ formation branching ratio values in Table 5 are for 297 – 300 K and 735 – 760 torr with the exception of the study by Chow et al. (2003) at 100 torr. $RONO_2$ formation branching ratios were determined by Atkinson et al. (1982b) for $EtONO_2$, and the combination of the 1- and 2-$RONO_2$ isomers for the C_3-C_5 $RONO_2$ from photooxidation experiments with mixtures of NO_x and n-alkanes using OH as the oxidation initiator. The $EtONO_2$ branching ratio from this study will be discussed below. Yields of $RONO_2$ and the $RONO_2$ formation branching ratio was calculated from $\Delta[RONO_2]/\Delta$[n-alkane]. The $RONO_2$ formation branching ratio is equal to the rate constant ratio of the RO + NO_2 product channels – *i.e*. $k_{3b}/(k_{3b}+k_{3a})$. The $RONO_2$ formation branching ratios for the C_3-C_5 RONO2 were derived from the sum of the 1- and 2-$RONO_2$ isomer yields. Atkinson et al. (1983) updated the 2-$PeONO_2$+3-$PeONO_2$ branching ratio from 0.117 ± 0.019 at 299 K and 735 torr in the previous study to 0.125 ± 0.003 via temperature and pressure dependent yield experiments. Atkinson et al. (1983) account for pressure and temperature dependent $RONO_2$ yields from secondary C_5-C_8 $RONO_2$ yields observed in Atkinson et al. (1982b) and Atkinson et al. (1983) using a generalized falloff equation determined from nonlinear least-squares fits to the C_5-C_8 $RONO_2$ yields. This equation produces the C_3-C_5 $RONO_2$ yields in Table 2 (Atkinson et al., 1983), which agree well with the observed yields.

Atkinson et al. (1984a) calculated individual isomeric $RONO_2$ yields and formation branching ratios from previous experiments (Atkinson et al., 1982b; Atkinson et al., 1983). Atkinson and coworkers devised a partial rate constant method to determine the H-atom abstraction branching ratios for alkanes by comparing calculated alkane + OH rate coefficients from alkane + OH structure-activity relationships to experimentally determined alkane + OH rate coefficients (Atkinson et al., 1982a; Atkinson et al., 1984b). These H-atom abstraction branching ratios were then applied to the branching ratios derived from the summed $RONO_2$ yields to determine the isomeric yields. Carter and Atkinson (1985) provided updated H-atom abstraction branching ratios from an updated partial rate constant estimation method based on further experiments of alkane + OH reactions (Atkinson, 1986). These updated values provided new isomeric $RONO_2$ formation branching ratios (Atkinson et al., 1982b; Atkinson et al., 1983). The only notable changes in the isomeric $RONO_2$ formation branching ratios from the updated H-atom abstraction branching ratios were increases from 0.129 ± 0.016 to 0.134 ± 0.016 for 2-$PeONO_2$ and 0.131 ± 0.016 to 0.146 ± 0.016 for 3-$PeONO_2$. Atkinson et al. (1987) added temperature and pressure

dependent formation experiments of C_5-C_6 branched alkanes, applying the same temperature and pressure dependent falloff equation from Atkinson et al. (1983) and Carter and Atkinson (1985) to determine the relative formation relationship between primary and tertiary $RONO_2$ to their secondary counterparts. Atkinson et al. 1987 thus found that the $RONO_2$ formation branching ratios for primary and tertiary isomers were 0.37 and 0.41 of the secondary isomer branching ratio (Atkinson et al., 1987). The 2-$PrONO_2$, 2-$BuONO_2$, and 2-$PeONO_2$ branching ratios in Table 2 from Atkinson et al. (1987) were calculated with the falloff expression and parameters within the reference, while the 1-$PrONO_2$ value was calculated as 0.37 of the reported 2-$PrONO_2$ value.

Arey et al. (2001) updated $RONO_2$ formation branching ratios (Table 5). Isomeric yields and individual formation branching ratios for 2-$PrONO_2$ and 2-$BuONO_2$ were recalculated from previous summed $RONO_2$ yields (Atkinson et al., 1982b) with improved structure-activity relationship derived partial rate constant calculations from Kwok and Atkinson (1995). The 1-$PrONO_2$ branching ratio in Arey (2001) (row of Table 5) is calculated as 0.4 of the 2-$PrONO_2$ value per recommendation by Carter and Atkinson (1989). Arey et al. (2001) also reported new branching ratios for 2-$PeONO_2$ and 3-$PeONO_2$ (0.106 ± 0.018 and 0.126 ± 0.018 respectively) from OH initiated reactions of n-pentane in the presence of NO (Arey et al., 2001; Carter and Atkinson, 1989). We note that the 2-$PeONO_2$ branching ratio of 0.106 ± 0.018 is on the lower end of previously reported experimental 2-$PeONO_2$ value range (Atkinson et al., 1984a; Carter and Atkinson, 1985). Aschmann et al. (2006) provided an additional update to the 2-$PeONO_2$ and 3-$PeONO_2$ branching ratio values with a pressure dependence study of 2-$PeONO_2$ and 3-$PeONO_2$ formation from OH radical initiated n-pentane oxidation in the presence of NO experiments. Aschmann et al. (2006) reported 2-$PeONO_2$ and 3-$PeONO_2$ branching ratios of 0.096 ± 0.009 and 0.116 ± 0.009 respectively. Both values are at the lower range of the previously reported branching ratio ranges (Arey et al., 2001; Atkinson et al., 1984a; Carter and Atkinson, 1985). Cassanelli et al. (2007) reported the temperature dependence of 2-$PeONO_2$ formation at 760 torr, and observed a 2-$PeONO_2$ branching ratio of 0.11 ± 0.02, which is in agreement with the growing range of previous values.

The number of studies reporting $MeONO_2$ and $EtONO_2$ is much smaller than the other $RONO_2$ of interest here as a result of the difficulty in detecting $MeONO_2$ or $EtONO_2$ in the controlled kinetics chamber and reactor experiments. Specifically, the detection of $MeONO_2$ above the signal-to-noise threshold of the employed detector in such an experiment was not realized until 2012 (Butkovskaya et al., 2012). Flocke et al. (1998) estimated a $MeONO_2$ branching ratio range of $1.5\text{-}3\times10^{-4}$ in the lower troposphere as a 3-fold increase from the value of $0.5\text{-}1\times10^{-4}$ that was constrained by $MeONO_2$ measurements in the lower stratosphere. Scholtens et al. (1999) were unable to detect $MeONO_2$ above the detection limit of their system, and thus estimated an upper limit $MeONO_2$ branching ratio of <0.03 at 298 K and 100 torr from the lack of $MeONO_2$ detection in a CH_4 + NO oxidation experiment in a flow tube reactor system. Butkovskaya et al. (2012) reported the first temperature and pressure dependent $MeONO_2$ branching ratio over the ranges of 50-500 torr and 223-300 K from the direct detection of $MeONO_2$ in a turbulent flow reactor. The relationship between $MeONO_2$ formation branching ratios and pressure (50-500 torr) yields a linear pressure dependence that can be extrapolated to 760 torr. A branching ratio value of 0.011 ± 0.001 was calculated for 760 torr and 298 K.

Atkinson et al. (1982b) report an upper limit $EtONO_2$ branching ratio of ≤0.014 from their Cl-atom initiated oxidation of ethane in the presence of NO at 299 K and 235 torr. The upper limit designation was applied as a result of the theory that the ethyl alkoxy radical + NO recombination reaction could be increasing the observed $EtONO_2$ yield. Butkovskaya et al. (2010) reported the

temperature (223-298 K) and pressure (100-600 torr) dependence of the $EtONO_2$ branching ratio, and extrapolated these data to solve for a branching ratio value of 0.03 ± 0.01 at 298 K and 760 torr (Butkovskaya et al., 2010).

2. Temperature and pressure dependent $RONO_2$ formation branching ratio calculations

Temperature and pressure dependent secondary C_3-C_5 $RONO_2$ formation branching ratios (summarized in Table S2) are calculated for average daytime winter 2011 (278 K), spring 2015 (285 K), and summer 2015 (298 K) temperature conditions. An atmospheric pressure of 0.82 atm (620 torr) is used to calculate [M]. [a]Units of [M] are in molecules cm^{-3}. The C_3-C_5 branching ratios are calculated with a falloff expression developed by Carter and Atkinson (1989). Details of the evolution of falloff expression are provided in supplemental section 1. The equations are detailed below (SI E1-E3);

$$\frac{k_{3b}}{k_{3a}} \; or \; \frac{k_{3b}}{k_{3a}+k_{3b}} = \left[\frac{Y_O^{298\ or\ 300}[M]\left(\frac{T}{298\ or\ 300}\right)^{-m_O}}{1+\frac{Y_O^{298\ or\ 300}[M]\left(\frac{T}{298\ or\ 300}\right)^{-m_O}}{Y_\infty^{298\ or\ 300}\left(\frac{T}{298\ or\ 300}\right)^{-m_\infty}}} \right] F^z \qquad \text{(SI E1)}$$

where

$$z = \left(1 + \left[log\left(\frac{Y_O^{298\ or\ 300}[M]\left(\frac{T}{298\ or\ 300}\right)^{-m_O}}{Y_\infty^{298\ or\ 300}\left(\frac{T}{298\ or\ 300}\right)^{-m_\infty}} \right) \right]^2 \right)^{-1} \qquad \text{(SI E2)}$$

and

$$Y_\infty^{298\ or\ 300} = \alpha e^{\beta n} \qquad \text{(SI E3)}$$

$Y_O^{298\ or\ 300}[M]$ and $Y_\infty^{298\ or\ 300}$ are the limiting low-pressure and high-pressure rate constant ratios of k_{3b}/k_{3a} for 298 or 300 K. Carter and Atkinson (1989) use 300 K and Arey et al. (2001) use 298 K, which is reflected in the '298 or 300' option in the above equations. The third body concentration ([M]) is calculated from the ideal gas law for each season's daytime average temperature at an atmospheric pressure of 0.82 atm, which is representative of the BAO site. Values of α, β, *F*, m_o, and m_∞ are parameters determined from fitting equation SI E1 to experimentally derived $RONO_2$ branching ratios for $RONO_2$ with different numbers of carbon (n). The values of the parameters derived from the fitted branching ratios that were used for the calculations in Table S2 are provided in Table 4.

Pressure and temperature dependent branching ratios for $EtONO_2$ (summarized in Table S2) are calculated for the local atmospheric pressure and seasonal temperatures detailed above with SI E4 from Butkovskaya et al. (2010),

$$\beta(P,T)\% = \left((3.88 \times 10^{-3}) \times P_{torr} + 0.365\right) \times \left(1 + 1500\left(\frac{1}{T} - \frac{1}{298}\right)\right) \quad \text{(SI E4)}$$

where P_{torr} is atmospheric pressure in torr and T is temperature in Kelvins. Butkovskaya et al. (2012) report a pressure dependence of the $MeONO_2$ branching ratio over a 50 – 500 torr range at 298 k, and temperature dependence over 223 – 300 K at 100, 150, and 200 torr. Equation S2 can be used to extrapolate the $MeONO_2$ branching ratio to 620 torr for this study (Butkovskaya et al., 2012),

$$\beta(P)(\%) = (1.03 \pm 0.04) \times 10^{-3}(P_{torr}) + (0.29 \pm 0.01)) \quad \text{(SI E5)}$$

which yields a branching ratio of 0.93 ± 0.05 %. There is a reported 34% decrease in the $MeONO_2$ formation branching ratio from 279 K to 298 K at 200 torr (Butkovskaya et al., 2012). Extrapolating this temperature dependence to 620 torr may not be appropriate.

3. J_{RONO2} value determinations

Seasonal photolysis rates (J_{RONO2}) for $MeONO_2$, $EtONO_2$, 1-$PrONO_2$, and 2-$BuONO_2$ were calculated with the National Center for Atmospheric Research Quick TUV calculator (http://cprm.acom.ucar.edu/Models/TUV/Interactive_TUV/_)(Madronich et al., 1998). The model was initiated with the longitude and latitude of the Boulder Atmospheric Observatory (BAO) in Erie, CO (40, -105), and an elevation of 1.56 km asl. Seasonal J_{RONO2} values were calculated every 2 hours from 08:00 – 18:00. For the NACHTT Winter 2011 campaign J_{RONO2} values were generated for March 1, 2011. For the SONGNEX Spring 2015 campaign J_{RONO2} values were generated for April 1, 2015 and May 1, 2015. For the Summer 2015 campaign J_{RONO2} values were generated for July 1, 2015 and August 1, 2015. Two dates, one near the beginning and end of the campaign, were chosen for a better representation of the longer SONGNEX field campaigns. Average and standard deviation J_{RONO2} values were calculated from the 08:00 – 18:00 J_{RONO2} values for the single day for NACHTT, and both days for the SONGNEX campaigns. The range of J_{RONO2} values reported in Table 3 were generated as the average ± standard deviation for each campaign.

The TUV calculator does not report J_{RONO2} values for 2-$PrONO_2$, 2-$PeONO_2$, and 3-$PeONO_2$. However, the TUV calculator outputs the actinic flux for an atmospherically relevant wavelength range. The photolysis rates for 2-$PrONO_2$, 2-$PeONO_2$, and 3-$PeONO_2$ were calculated with the following expression;

$$J_{RONO_2} = \int_{\lambda_{min}}^{\lambda_{max}} I(\lambda)\sigma(\lambda)\Phi(\lambda)d\lambda \quad \text{(SI E6)}$$

where I(λ) is the actinic flux at wavelength λ, σ(λ) is the absorption cross-section at wavelength λ, and Φ(λ) is the photodissociation quantum yield at wavelength λ. Absorption cross-sections for 2-$PrONO_2$ were taken from Talukdar et al. (1997a). Absorption cross-sections for 2-$PeONO_2$ were taken from Roberts and Fajer (1989). Because the 3-$PeONO_2$ absorption cross-sections are not reported in the literature, the absorption cross-sections for 2-$PeONO_2$ were used for 3-$PeONO_2$. The photodissociation quantum yields were assumed to be unity (Roberts and Fajer, 1989; Talukdar et al., 1997a).

Uncertainties are not reported from the TUV calculator. We took the uncertainty to be the RSD of each seasonal daytime (08:00 – 18:00) J_{RONO2} average. The uncertainty is reported as the range of J_{RONO2} for each campaign in Table 3.

4. Deposition calculations

Flux and dry deposition velocities (V_d) were estimated from a simplification of the following mass balance equation (SI E7) (Russo et al., 2010; Swarthout et al., 2013).

$$\frac{d[X_{BL}]}{dt} = \frac{ER}{H} + P - k_{OH}[OH][X_{BL}] - \frac{V_e}{H}(X_{BL} - X) - J_X + Advection \quad \text{(SI E7)}$$

where $d[X_{BL}]/dt$ is the change in concentration of X in the boundary layer during time (t), ER/H is the emissions rate of X in a boundary layer depth of H, P is the production rate of X, $k_{OH}[OH][X_{BL}]$ is the loss of X to oxidation by OH, V_e/H is the vertical transfer coefficient of X in a boundary layer depth of H, which is scaled by the difference in X_{BL} and X in the mixed layer aloft, and J_x is the photolysis rate of X at the surface. By choosing a nighttime period for these calculations the chemical production, loss to OH, and photolysis terms go to zero. Loss to nighttime oxidants such as O_3 and NO_3 is negligible (Roberts, 1990; Talukdar et al., 1997a; Talukdar et al., 1997b). Advection and vertical mixing is assumed to be negligible when a stable nocturnal boundary layer forms and wind speeds are low. Under such cases the mass balance equation reduces to SI E8.

$$\frac{d[X_{BL}]}{dt} = \frac{ER}{H} \quad \text{(SI E8)}$$

Outside of sites impacted by oceanic emissions or fresh biomass burning plumes, the direct emissions of $RONO_2$ do not contribute to ambient $RONO_2$ mixing ratios. The emission ratio can be replaced with flux by rearranging to SI E9;

$$\frac{d[X_{BL}]}{dt} \cdot H = Flux \quad \text{(SI E9)}$$

Flux of $RONO_2$ were estimated from the nighttime decay rate of alkyl nitrates (change in concentration over given time, pptv/s) multiplied by the nocturnal boundary layer height for nights with surface wind speeds under 4 m/s, and when $RONO_2$ exhibited decreasing mixing ratios between 22:00 and 06:00 with an r^2 of ≥0.50 between mixing ratio and time (Fig. S1a). Dry deposition velocity is then calculated with SI E10 (Russo et al., 2010);

$$V_d = \frac{Flux}{-C} \quad \text{(SI E10)}$$

where C is the mean $RONO_2$ mixing ratio during the flux period.

Fixed-height meteorological measurements of temperature and wind speed were continuously made at the BAO site at 10, 100, and 300 meter heights for all campaigns (Fig. S2c). During the winter 2011 campaign, additional time-resolved vertical profiles of potential temperature and wind speed were made on a moveable carriage on the 300 m tower (Fig. S2b). These higher resolution temperature measurements allowed us to determine nights with a stable nocturnal boundary layer (*i.e.* potential temperature inversions and stratified wind speeds). This flux and depositional velocity estimation technique was successfully used by Russo et al. (2010) at a rural site in New Hampshire. The rural New Hampshire site was characterized as commonly forming stable nocturnal boundary layers with low wind speeds and O_3 depletion at night (Russo et al., 2010). Nights when $MeONO_2$ exhibited a decrease in concentration with windspeeds <0.5 m/s and O_3 < 5 ppbv (indicative of O_3 depletion from dry deposition) were used to calculate $MeONO_2$ fluxes and deposition velocities. Nights during winter 2011 at the BAO site rarely experienced surface windspeeds < 3 m/s and O_3 depletion. However, during 22:00

06 March 2011 – 06:00 07 March 2011 we note that a stable boundary layer likely formed with a ceiling at 150 m from a slight potential temperature inversion (Fig. S2b). Decreases in $RONO_2$ concentration occur through the night (Fig S2a). The average surface wind speed during 22:00 06 March 2011 – 06:00 07 March 2011 is 4 m/s, which is larger than the 0.5 m/s cutoff of (Russo et al., 2010). The winter 2011 nighttime wind speeds at BAO are consistently greater than 0.5 m/s, thus some of the $RONO_2$ decay could be attributed to advection. An estimated boundary layer height of 150 m agrees with previous estimates of stable nocturnal boundary layer heights of 120 ± 50 m during winter 2011 at BAO (VandenBoer et al., 2013). Flux and dry deposition velocities scale with boundary layer height (Russo et al., 2010), without collocated boundary layer height measurements, the values in Table S7 should be considered estimates.

Seasonal dry deposition rate coefficients (k_{dep}, s^{-1}) were calculated with SI E11;

$$k_{dep} = \frac{V_d}{H} \quad \text{(SI E11)}$$

where H is the average boundary layer height for each season. Average boundary layer heights of 375, 750, and 1500 m were used for winter, spring, and summer respectively. Winter and summer heights were estimated from previous studies in the region.(Haagenson, 1979; Halliday et al., 2016; Neff, 1997; Schneider and Lilly, 1999)

5. $MeONO_2$ k_A and k_B uncertainties

The preferred rate coefficient for CH_4+OH from the IUPAC Task Group On Atmospheric Chemical Kinetic Data has an error of 1% for the ambient temperature range during the spring 2015 and summer 2015 campaigns (IUPAC, 2017). The preferred $MeONO_2$+OH rate coefficient has an uncertainty of 22% at 298 K (IUPAC, 2017). Uncertainties for the average spring 2015 daytime J_{RONO2} for $MeONO_2$ and 2-$BuONO_2$ are 61 and 67%, respectively. The uncertainties in J_{RONO2} selection have a negligible impact on the agreement between modeled and measured $RONO_2$/RH.

Supplemental tables.

Table S1. OH + alkane H-atom abstraction branching ratio

RONO2	Parent alkane	α_1[1]
MeONO2	Methane	1
EtONO2	Ethane	1
1-PrONO2	Propane	0.26
2-PrONO2	Propane	0.74
2-BuONO2	n-butane	0.87
2-PeONO2	n-pentane	0.57
3-PeONO2	n-pentane	0.35

[1](Kwok and Atkinson, 1995). Values of α_1 are calculated for 298 k and 760 torr.

Table S2. Calculated temperature and pressure dependent C_3-C_5 $RONO_2$ formation branching ratios

Season		winter 2011			spring 2015			summer 2015		
Carbon number		3	4	5	3	4	5	3	4	5
[M][c]			2.15			2.09			2.00	
Temp.[d]			278			285			298	
$RONO_2$ branching ratios	Arey 2001[1]	0.048	0.087	0.142	0.044	0.079	0.127	0.038	0.064	0.104
	Carter 1989[2,a]	0.052	0.108	0.19	0.049	0.099	0.169	0.044	0.084	0.137
	Carter 1989[2,b]	0.056	0.103	0.17	0.05	0.092	0.152	0.042	0.076	0.125
	Average	0.052	0.099	0.17	0.048	0.09	0.15	0.041	0.075	0.12
	Std. Deviation	0.003	0.009	0.02	0.003	0.008	0.02	0.002	0.008	0.01
	% deviation	0.06	0.09	0.12	0.06	0.09	0.12	0.06	0.11	0.11

[1](Arey et al., 2001), [2](Carter and Atkinson, 1989). [c]Units of [M] are in molecules cm^{-3}. [d]Units of temperature are in Kelvins. [a,b]Two sets of parameter values are provided in Carter and Atkinson (1989), which are provided in Table S4 below. Details of the $RONO_2$ formation branching ratios are provided in section 1 of this supplemental.

Table S3. Calculated temperature and pressure dependent $EtONO_2$ and pressure dependent $MeONO_2$ formation branching ratios.

		Seasonal $RONO_2$ branching ratios		
$RONO_2$	Reference	winter 2011	spring 2015	summer 2015
$MeONO_2$	Butkovskaya 2012[1]		0.0093 ± 0.0005	
$EtONO_2$	Butkovskaya 2010[2]	0.038	0.034	0.028

[1](Butkovskaya et al., 2012), [2](Butkovskaya et al., 2010). An explanation for the calculations of seasonal $MeONO_2$ and $EtONO_2$ branching ratios are provided in section 1 of the supplemental.

Table S4. Equation SE1-SE3 parameters used to calculate temperature and pressure dependent C_3-C_5 $RONO_2$ formation branching ratios

	α	β	F	m_o	m_∞	$Y_\infty^{298\ or\ 300}$
Arey 2001[1]	2.00	1	0.41	0	8	0.43
Carter 1989[2.a]	1.95	0.947	0.556	2.99	4.69	0.435
Carter 1989[2,b]	1.94	0.97	0.411	0	8.1	0.826

[1](Arey et al., 2001), [2](Carter and Atkinson, 1989). [a,b]Two sets of parameter values are provided in Carter and Atkinson (1989).

Table S5. Average alkyl nitrate parent alkane mixing ratios (ppb_v) at BAO.

Parent alkane	winter 20111	spring 20152	summer 20152
	Average mixing ratios (standard deviation), ppb_v		
Methane*		2 (0.1)	2 (0.1)
Ethane	22 (22)	16 (22)	23 (33)
Propane	16 (19)	9 (13)	8 (11)
n-Butane	7 (9)	2 (3)	4 (6)
n-Pentane	2 (2)	1 (2)	3 (5)

[1](Swarthout et al., 2013), [2](Abeleira et al., 2017). *Methane was not measured during winter 2011.

Table S6. Seasonal lifetime ranges in days of C_1-C_5 $RONO_2$ at the BAO site in respect to OH oxidation ($\tau_{OH} = 1/k_4$), photolysis ($\tau_{hv} = 1/J_5$), and OH + photolysis ($\tau_{OH+hv} = 1/k_B$)**.**

	Lifetimes								
AN	τ_{OH} - Winter 2011	τ_{OH} - Spring 2015	τ_{OH} - Summer 2015	τ_{hv} - Winter 2011	τ_{hv} - Spring 2015	τ_{hv}- Summer 2015	τ_{OH+hv} - Winter 2011	τ_{OH+hv} - Spring 2015	τ_{OH+hv} - Summer 2015
$MeONO_2$	174-524	98-243	54-108	23-165	15-61	12-39	18-105	12-43	9-25
$EtONO_2$	20-60	12-29	7-13	14-105	9-36	8-24	8-35	5-15	4-9
1-$PrONO_2$	7-22	4-11	2-5	10-68	6-25	6-17	4-15	2-7	2-4
2-$PrONO_2$	14-41	8-20	5-10	12-77	7-28	7-18	6-26	4-11	3-6
2-$BuONO_2$	4-13	3-6	2-3	12-98	7-38	6-24	3-12	2-6	1-3
2-$PeNONO_2$	2-6	1-3	0.8-1.5	14-115	9-43	6-24	2-6	1-3	0.7-1.5
3-$PeONO_2$	3-10	2-5	1-3	15-145	9-43	6-24	3-10	2-5	1-2

241 **Table S7.** Fluxes and dry deposition velocities calculated from 22:00 06 March 2011 – 06:00 07 March 2011.

$RONO_2$	$d[RONO_2]/dt$	C	Flux	V_d	R^2
$MeONO_2$	-0.3	4	-0.5	0.09	0.58
$EtONO_2$	-0.3	5	-0.5	0.08	0.48
1-$PrONO_2$	-0.2	3	-0.4	0.10	0.76
2-$PrONO_2$	-2.0	20	-4.0	0.15	0.67
2-$BuONO_2$	-3.4	30	-6.9	0.15	0.68
2-$PeONO_2$	-2.0	10	-5.2	0.15	0.68
3-$PeONO_2$	-1.1	8	-2.8	0.21	0.67

242 $d[RONO_2]/dt$ is the change in concentration of $RONO_2$ in the boundary layer between 22:00 06 March 2011 – 06:00
243 07 March 2011. C is the mean $RONO_2$ mixing ratio during the flux period in pptv. Flux is in units of nmol m^{-2} hr^{-1}.
244 Deposition velocity (V_d) is in units of cm s^{-1}.

Supplemental figures.

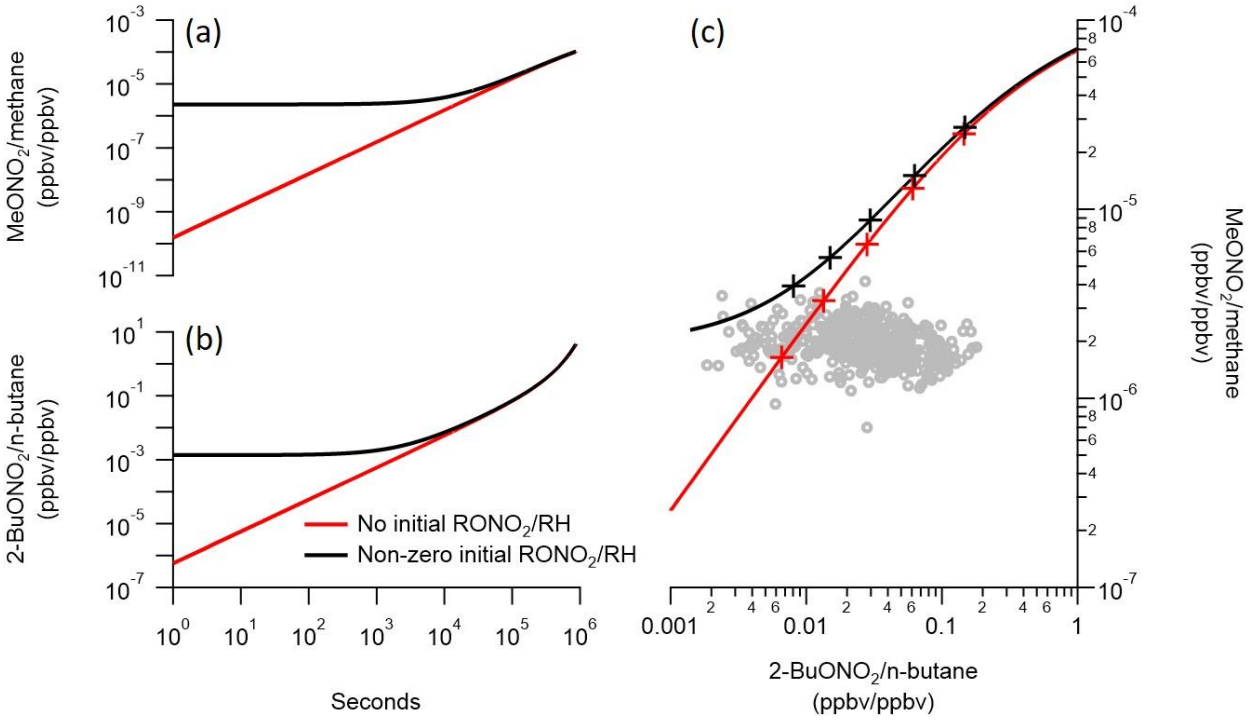

Figure S1. $RONO_2$/RH is modeled using E2 for (a) $MeONO_2$/methane and (b) 2-$BuONO_2$/n-butane using initial $RONO_2$/RH ratios of zero and non-zero values for spring 2015 conditions and branching ratios of 0.078 for 2-$BuONO_2$ and 0.0093 for $MeONO_2$. Non-zero $RONO_2$/RH initial ratios are defined as the 5th percentile of $RONO_2$/RH during morning (00:00 – 06:00) hours for spring 2015. (c) $MeONO_2$/methane is plotted against 2-$BuONO_2$/n-butane for the daytime (08:00 – 18:00) spring 2015 data. Observations are in grey circles, while model results are in lines with markers indicating photochemical age.

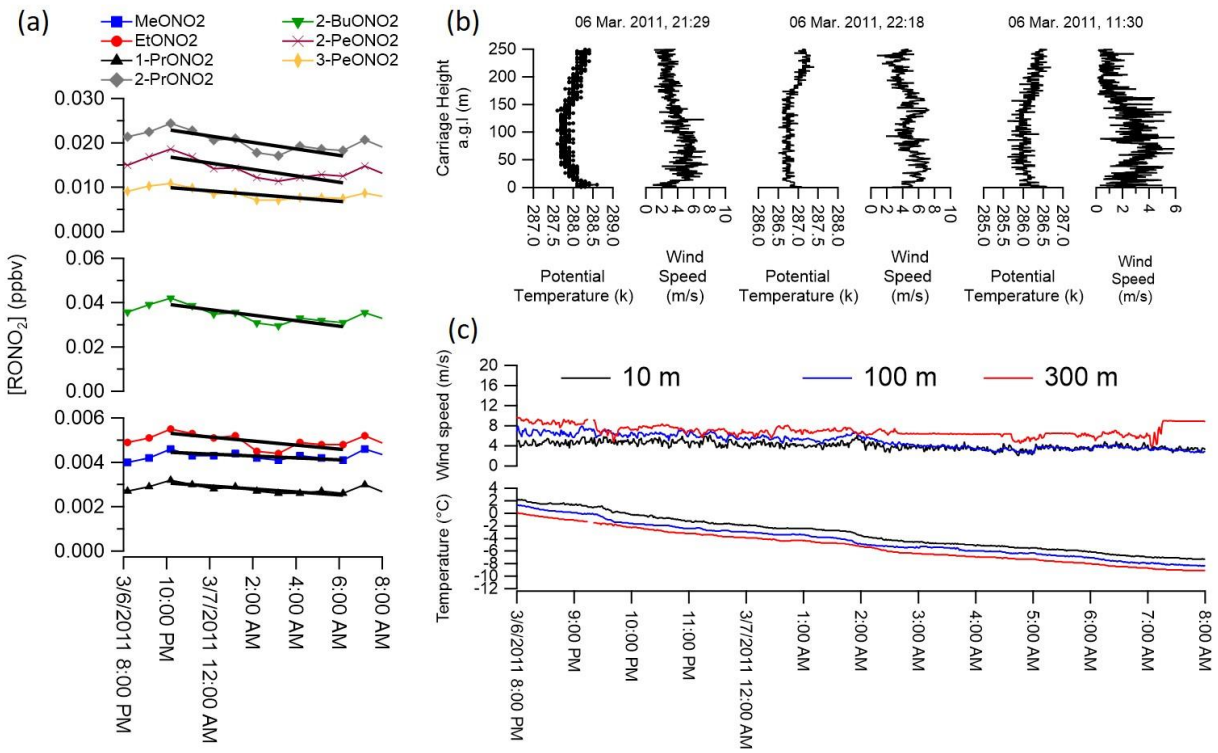

253

254 **Figure S2**. $RONO_2$ and meteorological data for dry deposition velocity calculations from the winter 2011
255 campaign for 06 March 2011 – 07 March 2011. (a) $RONO_2$ versus time for C_1 – C_5 $RONO_2$. (b) Individual
256 vertical profiles of potential temperature and wind speed that show the formation of a nocturnal
257 boundary layer ceiling at 22:18. (c) Temperature and wind speed measurements made at 10 m (black),
258 100 m (blue), and 300 m (red) on the tower at the BAO site.

259

260

261

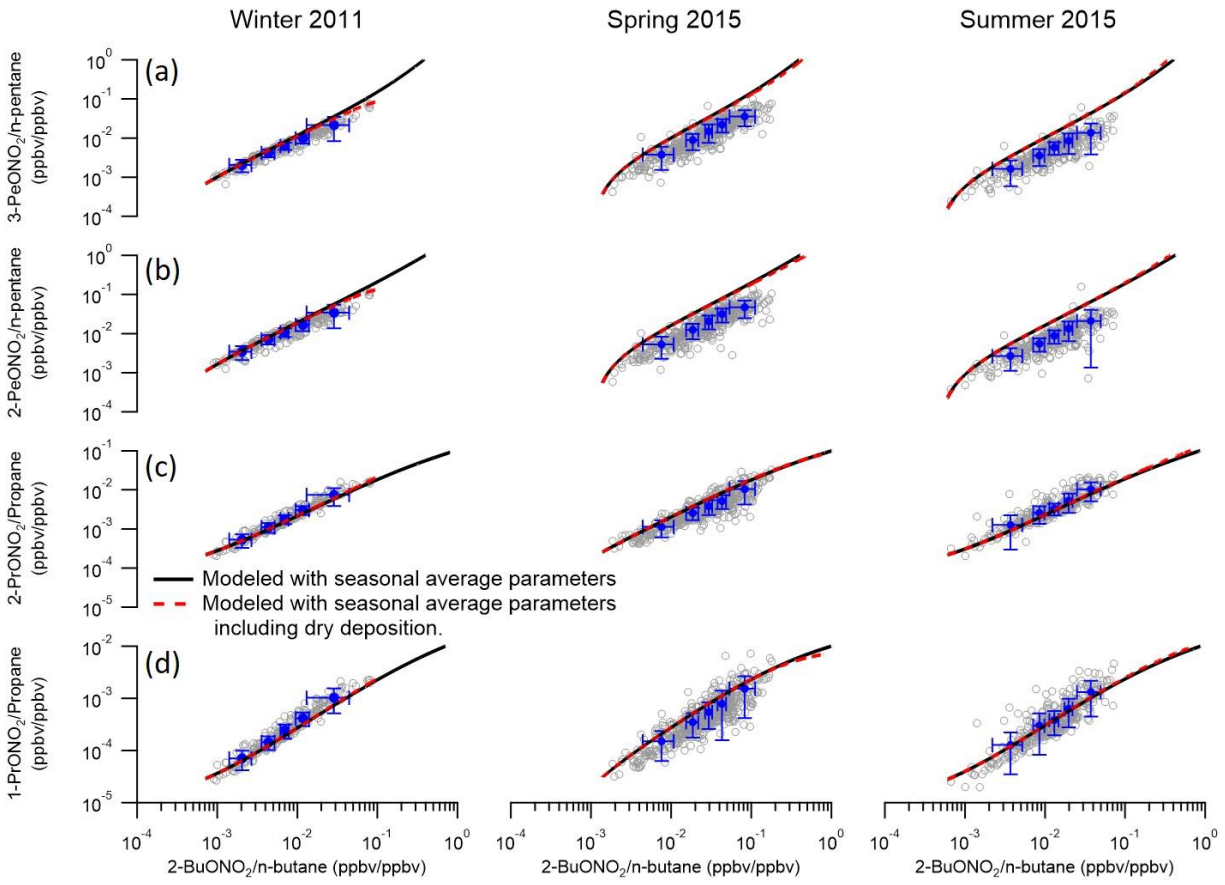

Figure S3. Observed daytime (08:00 – 18:00) $RONO_2/RH$ was plotted against 2-$BuONO_2$/n-butane (grey circles) for winter 2011 (left), spring 2015 (middle) and summer 2015 (right). Modeled $RONO_2/RH$ were generated with E2 using average campaign k_A, and k_B values from Table 2 and Table 3, and seasonal pressure and temperature dependent branching ratios (Table 1). Models were generated with non-zero initial ratios (black solid lines) defined as the 5th percentile value of $RONO_2/RH$ between 00:00 – 06:00 for all days during each respective campaigns. Dashed red lines are modeled $RONO_2/RH$ including loss by dry deposition (k_{dep}, Table S7. Solid blue circles are average $RONO_2/RH$ versus 2-$BuONO_2$/n-butane values with an equal number of points per averaging bin (n = 46 for winter 2011, 110 for spring 2015, and 69 for summer 2015). Error bars are one standard deviation of the $EtONO_2$/ethane and 2-$BuONO_2$/n-butane averages.

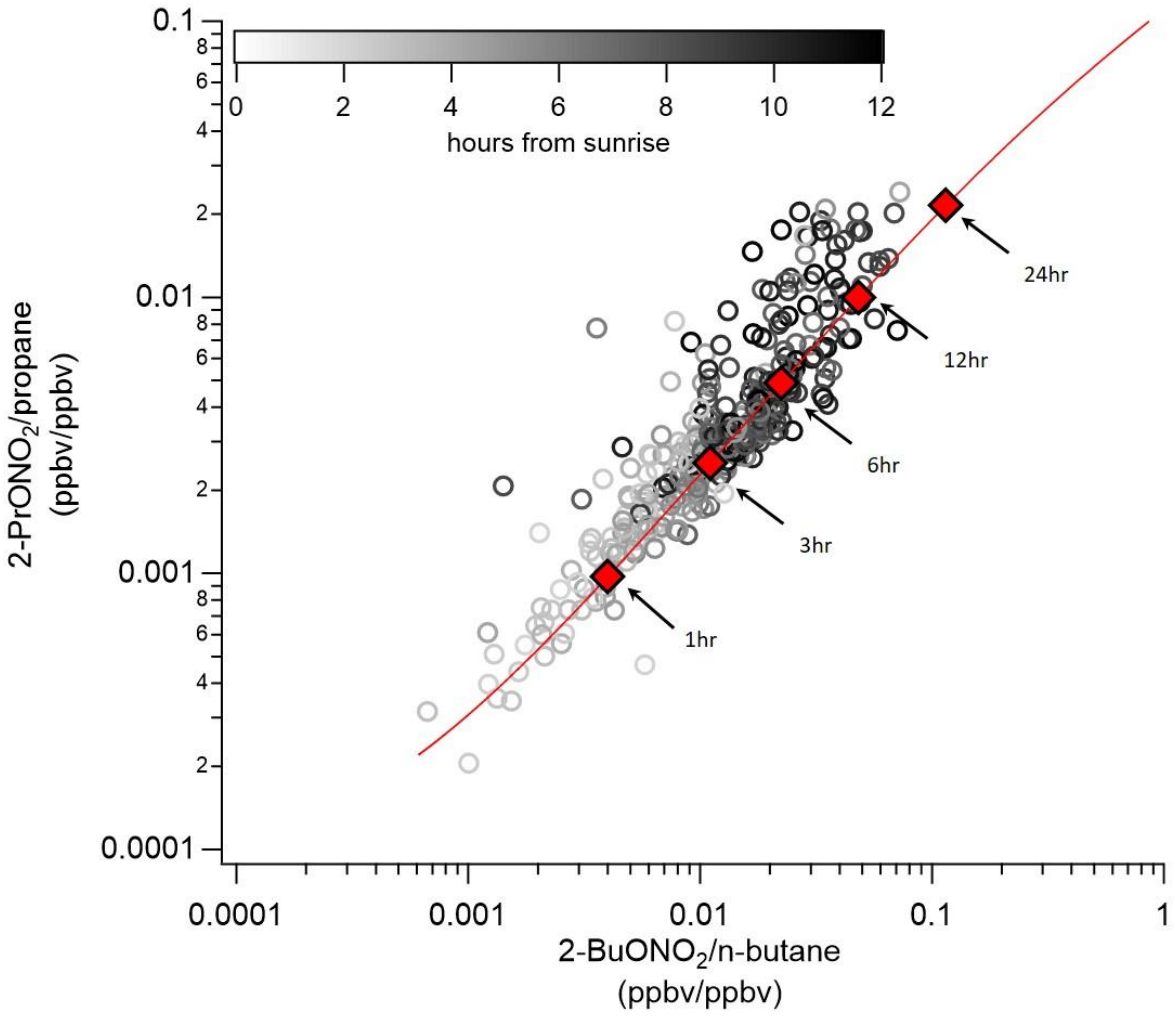

Figure S4. $RONO_2/RH$ is modeled using E2 for 2-$PrONO_2$/propane and 2-$BuONO_2$/n-butane. Branching ratios are averages from Table 1 ($\beta_{2\text{-PrONO2}}$ = 0.030; $\beta_{2BuONO2}$ = 0.068). Observed (circles) and modeled (line) 2-$PrONO_2$/propane are plotted against 2-$BuONO_2$/n-butane for the daytime (08:00 – 18:00) SONGNEX-summer data. Observations are colored by hours from sunrise for each data point. Markers for 1, 3, 6, 12, and 24 hours of photochemical aging for the two models are overlaid on the modeled curves.

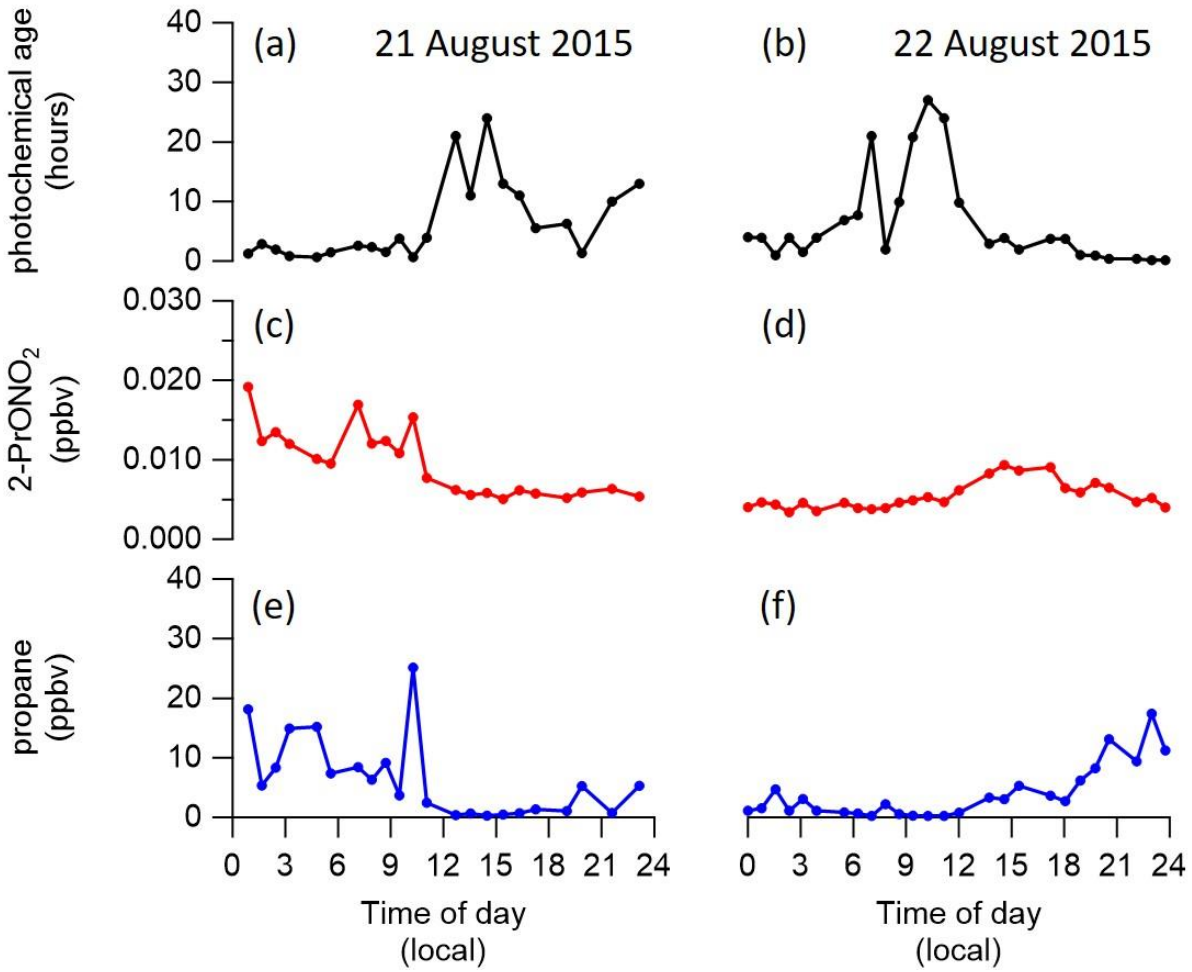

Figure S5. (a, b) Photochemical age, (c, d) 2-$PrONO_2$ concentration, and (e, f) propane concentration for 21 August 2015 and 22 August 2015 at the BAO site. Observed photochemical age is estimated by comparing ambient 2-$PrONO_2$/propane and 2-$BuONO_2$/n-butane values to modeled values.

Supplemental references.

Abeleira A, Pollack I, Sive B, Zhou Y, Fischer E, et al. 2017. Source characterization of volatile organic compounds in the Colorado Northern Front Range Metropolitan Area during spring and summer 2015. *J GEOPHYS RES-ATMOS* **122**(6): 3595-3613.

Arey J, Aschmann SM, Kwok ES, Atkinson R. 2001. Alkyl Nitrate, Hydroxyalkyl Nitrate, and Hydroxycarbonyl Formation from the NO_x− Air Photooxidations of C_5− C_8 n-Alkanes. *J PHYS CHEM A* **105**(6): 1020-1027.

Aschmann SM, Long WD, Atkinson R. 2006. Pressure dependence of pentyl nitrate formation from the OH radical-initiated reaction of n-pentane in the presence of NO. *J PHYS CHEM A* **110**(21): 6617-6622.

Atkinson R. 1986. Kinetics and mechanisms of the gas-phase reactions of the hydroxyl radical with organic compounds under atmospheric conditions. *CHEM REV* **86**(1): 69-201.

Atkinson R, Aschmann S, Carter W, Winer A, Pitts J. 1982a. Kinetics of the reactions of OH radicals with n-alkanes at 299±2 K. *INT J CHEM KINET* **14**(7): 781-788.

Atkinson R, Aschmann SM, Carter WP, Winer AM, Pitts JN. 1984a. Formation of alkyl nitrates from the reaction of branched and cyclic alkyl peroxy radicals with NO. *INT J CHEM KINET* **16**(9): 1085-1101.

Atkinson R, Aschmann SM, Carter WP, Winer AM, Pitts Jr JN. 1982b. Alkyl nitrate formation from the nitrogen oxide (NO_x)-air photooxidations of C_2-C_8 n-alkanes. *J PHYS CHEM-US* **86**(23): 4563-4569.

Atkinson R, Aschmann SM, Winer AM. 1987. Alkyl nitrate formation from the reaction of a series of branched RO_2 radicals with NO as a function of temperature and pressure. *J ATMOS CHEM* **5**(1): 91-102.

Atkinson R, Carter WP, Aschmann SM, Winer AM, Pitts JN. 1984b. Kinetics of the reaction of OH radicals with a series of branched alkanes at 297±2 K. *INT J CHEM KINET* **16**(4): 469-481.

Atkinson R, Carter WP, Winer AM. 1983. Effects of temperature and pressure on alkyl nitrate yields in the nitrogen oxide (NO_x) photooxidations of n-pentane and n-heptane. *J PHYS CHEM-US* **87**(11): 2012-2018.

Bertman SB, Roberts JM, Parrish DD, Buhr MP, Goldan PD, et al. 1995. Evolution of alkyl nitrates with air mass age. *J GEOPHYS RES-ATMOS* **100**(D11): 22805-22813.

Butkovskaya N, Kukui A, Le Bras G. 2010. Pressure and Temperature Dependence of Ethyl Nitrate Formation in the $C_2H_5O_2$ + NO Reaction. *J PHYS CHEM A* **114**(2): 956-964. doi:10.1021/jp910003a.

Butkovskaya N, Kukui A, Le Bras G. 2012. Pressure and Temperature Dependence of Methyl Nitrate Formation in the CH_3O_2 + NO Reaction. *J PHYS CHEM A* **116**(24): 5972-5980. doi:10.1021/jp210710d.

Carter WP, Atkinson R. 1985. Atmospheric chemistry of alkanes. *J ATMOS CHEM* **3**(3): 377-405.

Carter WP, Atkinson R. 1989. Alkyl nitrate formation from the atmospheric photoxidation of alkanes; a revised estimation method. *J ATMOS CHEM* **8**(2): 165-173.

Cassanelli P, Fox DJ, Cox RA. 2007. Temperature dependence of pentyl nitrate formation from the reaction of pentyl peroxy radicals with NO. *PHYS CHEM CHEM PHYS* **9**(31): 4332-4337.

Chow JM, Miller AM, Elrod MJ. 2003. Kinetics of the $C_3H_7O_2$ + NO Reaction: Temperature Dependence of the Overall Rate Constant and the i-$C_3H_7ONO_2$ Branching Channel. *J PHYS CHEM A* **107**(17): 3040-3047. doi:10.1021/jp026134b.

Flocke F, Atlas E, Madronich S, Schauffler S, Aikin K, et al. 1998. Observations of methyl nitrate in the lower stratosphere during STRAT: Implications for its gas phase production mechanisms. *GEOPHYS RES LETT* **25**(11): 1891-1894.

Haagenson PL. 1979. Meteorological and climatological factors affecting Denver air quality. *Atmospheric Environment (1967)* **13**(1): 79-85.
Halliday HS, Thompson AM, Wisthaler A, Blake DR, Hornbrook RS, et al. 2016. Atmospheric benzene observations from oil and gas production in the Denver-Julesburg Basin in July and August 2014. *J GEOPHYS RES-ATMOS* **121**(18): 11,055-11,074. doi:10.1002/2016JD025327.
IUPAC. 2017. Task Group on Atmospheric Chemical Kinetic Data Evaluation. Available at http://iupac.pole-ether.fr/. Accessed 9/14.
Kwok ES, Atkinson R. 1995. Estimation of hydroxyl radical reaction rate constants for gas-phase organic compounds using a structure-reactivity relationship: an update. *ATMOS ENVIRON* **29**(14): 1685-1695.
Madronich S, McKenzie RL, Björn LO, Caldwell MM. 1998. Changes in biologically active ultraviolet radiation reaching the Earth's surface. *J PHOTOCH PHOTOBIO B* **46**(1): 5-19. doi:https://doi.org/10.1016/S1011-1344(98)00182-1.
Neff WD. 1997. The Denver Brown Cloud studies from the perspective of model assessment needs and the role of meteorology. *J AIR WASTE MANAGE* **47**(3): 269-285.
Reeves CE, Slemr J, Oram DE, Worton D, Penkett SA, et al. 2007. Alkyl nitrates in outflow from North America over the North Atlantic during Intercontinental Transport of Ozone and Precursors 2004. *J GEOPHYS RES-ATMOS* **112**(D10).
Roberts JM. 1990. The atmospheric chemistry of organic nitrates. *ATMOS ENVIRON A-GEN* **24**(2): 243-287.
Roberts JM, Fajer RW. 1989. UV absorption cross sections of organic nitrates of potential atmospheric importance and estimation of atmospheric lifetimes. *ENVIRON SCI TECHNOL* **23**(8): 945-951.
Russo RS, Zhou Y, Haase K, Wingenter O, Frinak E, et al. 2010. Temporal variability, sources, and sinks of C_1-C_5 alkyl nitrates in coastal New England. *Atmos Chem Phys* **10**(4): 1865-1883.
Schneider JM, Lilly DK. 1999. An observational and numerical study of a sheared, convective boundary layer. Part I: Phoenix II observations, statistical description, and visualization. *J ATMOS SCI* **56**(17): 3059-3078.
Scholtens KW, Messer BM, Cappa CD, Elrod MJ. 1999. Kinetics of the CH_3O_2+ NO reaction: Temperature dependence of the overall rate constant and an improved upper limit for the CH_3ONO_2 branching channel. *J PHYS CHEM A* **103**(22): 4378-4384.
Simpson IJ. 2003. Photochemical production and evolution of selected C_2–C_5 alkyl nitrates in tropospheric air influenced by Asian outflow. *J GEOPHYS RES* **108**(D20). doi:10.1029/2002jd002830.
Sommariva R, Trainer M, de Gouw JA, Roberts JM, Warneke C, et al. 2008. A study of organic nitrates formation in an urban plume using a Master Chemical Mechanism. *ATMOS ENVIRON* **42**(23): 5771-5786.
Swarthout RF, Russo RS, Zhou Y, Hart AH, Sive BC. 2013. Volatile organic compound distributions during the NACHTT campaign at the Boulder Atmospheric Observatory: Influence of urban and natural gas sources. *J GEOPHYS RES-ATMOS* **118**(18): 10,614-10,637. doi:10.1002/jgrd.50722.
Talukdar R, Burkholder J, Gilles M, Roberts J. 1997a. Atmospheric fate of several alkyl nitrates Part 2: UV absorption cross-sections and photodissociation quantum yields. *CHEM SOC FARADAY T* **93**(16): 2797-2805.
Talukdar RK, Herndon SC, Burkholder JB, Roberts JM, Ravishankara A. 1997b. Atmospheric fate of several alkyl nitrates Part 1: Rate coefficients of the reactions of alkyl nitrates with isotopically labelled hydroxyl radicals. *CHEM SOC FARADAY T* **93**(16): 2787-2796.
VandenBoer TC, Brown SS, Murphy JG, Keene WC, Young CJ, et al. 2013. Understanding the role of the ground surface in HONO vertical structure: High resolution vertical profiles during NACHTT-11. *J GEOPHYS RES-ATMOS* **118**(17): 10,155-10,171. doi:10.1002/jgrd.50721.

Wang M, Shao M, Chen W, Lu S, Wang C, et al. 2013. Measurements of C_1–C_4 alkyl nitrates and their relationships with carbonyl compounds and O_3 in Chinese cities. *ATMOS ENVIRON* **81**: 389-398.
Worton DR, Reeves CE, Penkett SA, Sturges WT, Slemr J, et al. 2010. Alkyl nitrate photochemistry during the tropospheric organic chemistry experiment. *ATMOS ENVIRON* **44**(6): 773-785.